Available online at www.caspener.com

Caspian Journal of Energy

ISSN 0000-0000 (Print), **ISSN** 0000-0000 (Online)

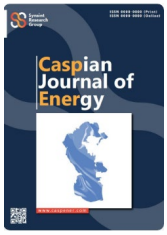

Research article

Formation processes of point defects in zirconium under the impact of neutrons in nuclear reactor conditions

A.A. Garibov *

Institute of Radiation Problems, Ministry of Science and Education Republic of Azerbaijan, Baku AZ-1143, Azerbaijan

ABSTRACT

In thermal energetic nuclear reactors with power parameters of 400–1200 MW, the recoil energy given to the nuclei and the energies of the scattered neutrons due to the elastic scattering of thermal and fast neutrons in the nuclear reactor materials were determined. Based on recoil energies, the rates of generation of point defects that can be formed in the example of zirconium metal and the parameters of diffusion and recombination processes have been determined.

KEYWORDS

Defects
Zirconium metal
Neutrons
Nuclear reactor
Recoil energies

OPEN ACCESS

1. Introduction

After the nuclear reactor accidents in Chernobyl and Fukushima, the safety problem in nuclear energy and technology has become especially important. Various aspects of this problem have been analyzed by the leading infrastructures and specialists of nuclear countries, the main reasons have been revealed, the scientific basis of safe nuclear reactors has been worked out, and real examples are already being applied. In nuclear energy reactors based on nuclear fission processes, the probability of an accident is mainly the occurrence of defects in nuclear reactor materials under the influence of factors such as high-energy radiation, particles, shrapnel, and temperature specific to the reactor environment. As a result, the materials lose their structural form and properties [1–15].

In the normal operating mode of nuclear reactors, materials are exposed to ionizing rays and particles under various conditions [16–20]. As a result of these processes, defects occur in the reactor materials, and in extreme cases, these factors show their effect. Therefore, it is of great importance to study the processes occurring in the nuclear reactor of thermal insulation material of nuclear reactors, the materials under the influence of radiation, particles, and temperature factors that exist in the normal operating mode of nuclear reactors and to characterize the defect cases that may arise as a result of them.

In the presented article, the processes of energization and defect formation of zirconium metal, which is the main component influence of neutrons released in the active zone of a water-cooled nuclear reactor, were theoretically studied [21–29].

2. Method

Research object. 99.9% pure zirconium was taken as the research object. Characteristic parameters of the processes of energy transfer to zirconium and defect formation were determined during the influence of neutrons under the conditions specific to water-cooled nuclear reactors [4, 5].

U235 was used as a fuel in the nuclear reactor (Tables 1–2). The energy distribution in MeV according to the fission products is given in Table 3.

Table 3 shows the values of nuclear densities of the most commonly used materials in the nuclear reactor [24, 25, 27].

Based on the given data and the theoretical data related to the interaction of the released energy carriers with metallic materials, the amount of energy given to zirconium metal as a result of these processes and the amount of point defects were evaluated.

* Corresponding author. *E-mail address:* adilgaribov@rambler.ru (A.A. Garibov)

Received 12 July 2024; Received in revised form 18 July 2024; Accepted 29 July 2024.

https://doi.org/10.53063/caspener.2024

Table 1. Parameters of VVER, PWR, BWR type nuclear reactors with potency of 440–1200 MW working with thermal neutrons [4, 5].

The average density of thermal neutrons in the active zone	2.7×10^{13}–4.4×10^{13} neutron/cm^2.s
The average density of fast neutrons in the active zone	1.9×10^{14}–4.0×10^{14} neutron/cm^2.s
The average density of fast neutrons	1×10^{14} neutron/cm^2.s
E_n > 0.1 MeV neutron influence (40 years)	5×10^{19}–1×10^{20} neutron/cm^2.s

3. Results and discussion

In reactors operating with thermal neutrons, the maximum distribution of U^{235} due to the energy of neutrons from fission products can be taken as approximately En ≈ 2 MeV [4–9, 23–25]. The maximum energy that can be given to the nuclei during the interaction of these neutrons with the above-mentioned nuclear reactor materials by the elastic scattering mechanism is determined by the following formula.

$$E_{repulsed}(max) = 4AE_n \cos^2\varphi / (1+A)^2 \quad (1)$$

where φ is the angle of recoil from the locations of the nuclei under the influence of neutrons and A is the mass of the nuclei entering the nuclear materials. During the report, the recoil angles φ = 0 ° and φ = 45 ° corresponding to the maximum and minimum values of the recoil energy were taken into account. The obtained results are presented in Table 4.

Energy loss of neutrons in nuclear reactor materials is characterized by the ξ average logarithmic decrement of energy [22–27].

$$\xi = \ln\frac{E_0}{E_1} = 1 + \frac{(A-1)^2}{2A}\ln\frac{A-1}{A+1} \quad (2)$$

Since the atomic masses of the elements included in the nuclear reactor materials are A > 10, the number of collisions to reduce the neutrons from E_0 = 2 MeV to the thermal state is empirically calculated with the following formula.

$$Z = \frac{18.2}{\xi} \quad (3)$$

The obtained results are given in Table 5.

We obtained values characterizing the average energy loss during neutron deceleration from E_0=2 MeV to E'=0.0253 eV with Eqs. 2 and 3.

Table 2. Values of the energy released as a result of the act of fission of the U^{235} nucleus.

Nucleus	U^{235}
The kinetic energy of the fragments, E_{frag}, MeV	166
Instant gamma quanta, $E_{\gamma,ins}$, MeV	7.2
Delayed gamma quanta, $E_{\gamma,del}$, MeV	7.2
The energy of neutrons, E_n, MeV	4.9
The energy of Beta particle, E_β, MeV	9.0
Anti neutrinos, E_ν, MeV	10

Table 3. Nuclear reactor materials and their nuclear residues.

The elements in the composition	$\frac{\rho}{A}$ ρ: density, g/cm^2; A: atomic mass	$N_i = \frac{\rho}{A}N_A$ N_A: Avogadro's number or Avagadro's constant, nucleus/cm^3
Be (beryllium)	0.205	1.27×10^{23}
Al (aluminum)	0.100	6.23×10^{22}
Fe (iron: ferrium)	0.140	8.72×10^{22}
Cd (cadmium)	0.076	4.73×10^{22}
Nb (niobium)	0.092	5.73×10^{22}
Zr (zirconium)	0.071	4.42×10^{22}

$$\bar{E} = \frac{E_0 - E_{ist}}{Z} \quad (4)$$

The energy given to the nuclei during the first or every collision was determined by Eq. 1.

The obtained results show that the recoil energy received by the nuclei during the first scattering from the nuclear reactor materials (Table 4) is higher than the average recoil energy (Table 5) determined based on the Eq. 4. The threshold energy $\bar{E}_{recoil}$ of removal of atoms from the crystal lattice sites in structural materials [4, 5, 25–27] can be determined approximately by the following equation:

$$E_h(atom) = 2.5E_d \quad (5)$$

where E_d is the bond energy in the structural lattice of atoms (E_d~40 eV). Therefore, the energy supplied to the structural material atoms during the neutron scattering process (Table 4) will be sufficient for their participation in the subsequent defect-formation processes.

One of the important factors in the process of defect formation under the influence of neutrons in reactor conditions is the free escape distance of neutrons in reactor materials. Free escape distances of neutrons due to absorption and scattering were calculated on the example of iron (Fe) and zirconium (Zr), which are widely used in structural materials. Based on the values of the macroscopic cross sections ($\sum i=\sigma_i.N_i$, $\sum i$: summation index) determined on the basis of microscopic cross sections of thermal and fast neutron absorption (σ_u) and scattering (σ_s) processes in these materials has been studied.

$$\lambda_i = \frac{1}{\sum i} \quad (6)$$

Table 4. Repulse energies that can be imparted to nuclei contained in nuclear reactor materials as a result of elastic scattering of neutrons.

Elements	**$E_{repulse}$(max) in eV at value of φ=0 °, cosφ=1**	**$E_{repulse}$(min) in eV at value φ=45 °, cosφ≈0.707**
Al (aluminum)	$2.75\cdot10^5$	1.37×10^5
Fe (iron: ferrium)	1.37×10^5	6.15×10^4
Cd (cadmium)	7.00×10^4	3.50×10^4
Nb (niobium)	8.42×10^4	4.21×10^4
Zr (zirconium)	8.60×10^4	4.29×10^4
Be (beryllium)	7.25×10^5	3.60×10^5

Table 5. Parameters of energy loss processes during scattering of neutrons with an energy of 2 MeV from nuclear reactor materials.

Isotopes of elements included in nuclear reactor materials	The energy of 2 MeV neutrons after scattering from nuclei, eV ($E' = \left(\frac{A-1}{A+1}\right).E_0$)	$\xi = 1 + \frac{(A-1)^2}{2A}\ln\frac{A-1}{A+1}$	$Z = \frac{18.2}{\xi}$	$\bar{E}_{repulse} = \frac{E_0 - E'}{Z}$
^{9}Be	1.28×10^{6}	0.546	34	5.89×10^{4}
^{27}Al	1.72×10^{6}	0.065	280	7.14×10^{3}
^{56}Fe	1.93×10^{6}	0.009	2022	9.89×10^{2}
^{91}Zr	1.96×10^{6}	0.013	1400	1.43×10^{3}
^{93}Nb	1.96×10^{6}	0.010	1820	1.10×10^{3}
^{112}Cd	1.96×10^{6}	0.002	9100	2.19×10^{2}

Free escape distances were determined with the above-mentioned equation (Table 6).

During the elastic scattering of neutrons from zirconium nuclei, the recoil energy given to the first scattered nuclei varies in the range of E_{recoil} =(4–8)×10^4 eV. The first scattered atoms (FSA) start displacement cascades by diffusion in the medium and new interaction with the atoms in the lattice nodes. Probabilities, times, and conditions of occurrence of these cascades are described in detail in Refs. [4–6]. When the energy of the first extracted atoms exceeds 40 kW, displacement cascades occur independently of each other in the form of sub-cascades [6]. Displacement cascades are divided into the following stages [4–6]:

-Stage I: Displacement, $\tau_I = 10^{-23} - 10^{-20}$ seconds.

-Stage II: Ballistic stage, $\tau_{II} = 10^{-16} - 10^{-13}$ seconds before collision between atoms.

-Stage III: Relaxation stage, $\tau_{III} \leq 10^{-10}$ seconds.

As can be seen in Table 6, the macroscopic cross-sections of thermal and fast neutron absorption processes in nuclear reactor materials containing Fe-56 and Zr-91 are much smaller than the microscopic cross-sections of scattering processes. Therefore, the free escape distance for both neutrons in these materials has been determined. An approximate comparison of the thicknesses (l) of structural parts based on Fe and Zr in nuclear reactors and the free escape distances (λ_s) of neutrons shows that both thermal and fast neutrons can be scattered only once in zirconium-based structural parts ($l_{thick}<\lambda_s$). During this scattering, depending on the scattering angle, the rate of formation of vacancy and internodal atoms in the structural material can be determined by taking into account the recoil energy $E_{recoil}\approx(4.3\div8.6)\times10^4$ eV given to the nucleus and the threshold energy for removing atoms from the lattice site:

$$W_{def}(i,V_i) = \Phi_n \cdot \frac{E_{recoil}}{E_h(atom)} \quad (7)$$

where, $W_{def}(i,V_i)$ is the defect formation rate and Φ_n is the flux density of fast neutrons.

During the scattering of thermal neutrons from zirconium nuclei, the recoil energy given to the nuclei E_{recoil} (thermal neutron) <4.5 eV, in defect formation processes, the values of the flux density of fast neutrons in nuclear reactors operating with thermal neutrons with a power of 400–1200 MW were taken into account, and Φ_n=(1.9–4.0)×10^{14} neutron/cm^2.s was taken [4–6]. The speed of defect processes on the surface of zirconium in a reactor with a power of 1200 MW is formed.

$$W_{def}(i,V_i)\approx(1.7–3.4)\times10^{17}\ atom/cm^2.s \quad (8)$$

In a thermal reactor with a power of 400 MW, $W_{def}(i,V_i)$ can vary in the following range of values.

$$W_{def}(i,V_i)=(0.82–1.63)\times10^{17}\ atom/cm^2.s \quad (9)$$

where i is metal atoms sliding between lattice nodes, V_i is their vacancy.

Due to the energy supplied to the zirconium nucleus as a result of the elastic scattering of neutrons, the process of defect formation can be shown schematically as follows:

$$-\underset{|}{\overset{|}{Me}}- \xrightarrow{n} -\underset{|}{\overset{|}{\boxed{V_i}}}- + Me_i(i) \quad (10)$$

After the first atomic output, the energy of the atoms will be as follows.

$$E' = E_0 - E_{threshold} \quad (11)$$

These atoms will cause diffusion and point collisions in the crystal structure. The diffusion of internodal atoms is expressed by the following formula.

$$D=D_0.\exp(-E_a/kT) \quad (12)$$

Table 6. Free escape distance due to the absorption and scattering processes of thermal and linear neutrons in iron and zirconium-containing materials.

Element	The macroscopic cross sections, $\sum i=\sigma_i.N_i$, 1/cm				$\lambda_{scattering} = \frac{1}{\sum scattering}$	
	For absorption processes		For scattering processes			
	Thermal neutrons	Fast neutrons	Thermal neutrons	Fast neutrons	Thermal neutrons	Fast neutrons
Fe-56	0.2224	0.009	0.9505	0.0741	1.05	19.49
Zr-91	0.0082	0.001	0.2846	0.0031	3.5	322.6

Table 7. Diffusion parameters of point radiation defects in Zr.

T (K)	$D=D_0.\exp(-E_a/kT)$, m^2/s	$L=\sqrt{D.\tau_I}$, nm		L_{II}/a	L_{III}/a
		$\tau_{II=10}^{-13}$ s	$\tau_{III=10}^{-10}$ s		
298	3.148×10^{-5}	0.56	5.61	1.55	4.29
573	3.266×10^{-5}	0.61	5.71	1.69	4.68

For zirconium, $D_0=3.4\times10^{-5}$ m^2/s, $E_a=1.98$ eV [4–6, 14]. During the impact of fast neutrons on the zirconium material, as a result of elastic scattering from the nuclei, due to the recoil energy provided by each neutron, approximately $N_d(i,Vi)=(4.3–8.6)\times10^2$. (i,V_i) pairs can be formed.

The internodal atoms and vacancies created according to Eq. 9 can be recombined according to the following processes [4, 5].

$$V_i + j \longrightarrow -\underset{|}{\overset{|}{Me}}- \text{(recombination)} \quad (13)$$

$$V_i, j + S \longrightarrow S \text{ (annihilation)} \quad (14)$$

where S is the defect flux.

Under the influence of neutrons, taking into account the creation of vacancies and atoms between lattice nodes in a stoichiometric ratio, in a simplified case, the rates of formation of defect pairs (V_i,j) can be expressed as follows.

$$\frac{dN_d}{d\tau} = (V_i, j) - \alpha N_d^2 \quad (15)$$

where τ and α are irradiation time and recombination constant [4, 14, 15].

$$\alpha=4\pi r_{IV}(D_i+D_v)\Omega \quad (16)$$

where D_i and D_v are diffusion constants of internodal atoms and vacancies; Ω is the volume of j-type point defects in m^3, and r_{IV} is the recombination radius, which is usually equal to the lattice constant α.

For simplicity, the vacancies can be assumed to be at rest relative to the internodal atoms. Taking point defects as spherical in internodal atomic dimensions, their volumes can be calculated by the expression $\Omega=4/3\pi r^3$.

For zirconium atoms, the value of the recombination constant can be approximately calculated using Eq. 15 based on the diffusion constant D_0, the activation energy E_a, and the lattice constant a = 0.361 nm. It should be noted that all calculations have been done by the author.

$$\alpha=8.35\times10^{15}\ s^{-1} \quad (17)$$

In water-cooled nuclear reactors with power parameters P=440–1200 MW we can see the dominance of recombination processes at any value of Nd by Eq. 14, the values of the rate of formation of point defects due to the elastic scattering of the neutrons as a result of the elastic scattering of the nuclei of zirconium metal element atoms determined based on the fast neutron flux density values and on the basis of their recombination constant values calculated.

The values of the diffusion constants of internodal atoms at T=298 K and 573 K were calculated based on Eq. 11 and the values of the possible displacement determined by the simplified expression are given in Table 7.

Conditionally, if we assume that the point defects formed under the influence of fast neutrons impacting every 1 cm^2 of metal surface mainly spread over the diffusion distance L within $\tau_{rk}=10^{-10}$ s the density of point defects $V=5.71\times10^{-7}$ cm^3 in the volume of the rectangular prism formed is approximately the following expression.

$$\left[N_d\right] = \frac{W(i,V).\tau_{rk}}{V} \approx 5.9\times10^{13}(i,V)/cm^3 \quad (18)$$

If we put the approximate values and α into Eq. 14, we can see that at T=573 K the processes of recombination of point defects go much faster than the processes of formation.

As can be seen from the Table 7, the subsequent collision processes of the first point defects cover a distance of 1.5–1.7 lattice constant in the temperature interval T=238–573 during the transfer time. During the relaxation time of point radiation defects, it crosses the lattice constant distance in the same temperature interval. The processes of interaction of point defects with biographical defects that may be present in zirconium are not followed in this paper. Point defects relaxed by these distances undergo recombination processes. Therefore, zirconium metal can be used for a long time in water-cooled thermal energy reactors [25, 29].

4. Conclusions

The processes of energy loss of neutrons and recoil energy given to atoms during elastic scattering with zirconium, a thermal insulation element material, in thermal and fast neutron fluences characteristic of thermal nuclear reactors with power parameters of 400 and 1200 MW have been theoretically studied.

Speeds of point defect formation processes, recombination constant of point defects in simplified versions, diffusion constant, and diffusion distances in the course of the processes taking place with their participation were evaluated due to the recoil energies given to metal atoms during the elastic scattering of neutrons. The obtained results can be used to explain the ability of zirconium to work in the field of long-term neutron influence in the active zone of a nuclear reactor.

CRediT authorship contribution statement

A.A. Garibov: Writing – original draft, Conceptualization, Investigation, Writing – review & editing.

Data availability

The data underlying this article will be shared on reasonable request to the corresponding author.

Declaration of competing interest

The authors declare no competing interests.

Funding and acknowledgment

The author would like to thank the doctoral students.

References

[1] L. Tavera-Davila, H.B. Liu, R. Herrera-Becerra, G. Canizal, M. Balcazar, J.A. Ascencio, Analysis of Ag Nanoparticles Synthesized by Bioreduction, J. Nanosci. Nanotechnol. 9 (2009) 1785–1791. https://doi.org/10.1166/jnn.2009.407.

[2] R. Ribeiro-Santos, D. Carvalho-Costa, C. Cavaleiro, H.S. Costa, T.G. Albuquerque, et al., A novel insight on an ancient aromatic plant: The rosemary (Rosmarinus officinalis L.), Trends Food Sci. Technol. 45 (2015) 355–368. https://doi.org/10.1016/j.tifs.2015.07.015.

[3] R. Motti, B. de Falco, Traditional Herbal Remedies Used for Managing Anxiety and Insomnia in Italy: An Ethnopharmacological Overview, Horticulturae. 7 (2021) 523. https://doi.org/10.3390/horticulturae7120523.

[4] V. Aleksic Sabo, P. Knezevic, Antimicrobial activity of Eucalyptus camaldulensis Dehn. plant extracts and essential oils: A review, Ind. Crops Prod. 132 (2019) 413–429. https://doi.org/10.1016/j.indcrop.2019.02.051.

[5] B. de Falco, L. Grauso, A. Fiore, G. Bonanomi, V. Lanzotti, Metabolomics and chemometrics of seven aromatic plants: Carob, eucalyptus, laurel, mint, myrtle, rosemary and strawberry tree, Phytochem. Anal. 33 (2022) 696–709. https://doi.org/10.1002/pca.3121.

[6] F. Brahmi, A. Abdenour, M. Bruno, P. Silvia, P. Alessandra, et al., Chemical composition and in vitro antimicrobial, insecticidal and antioxidant activities of the essential oils of Mentha pulegium L. and Mentha rotundifolia (L.) Huds growing in Algeria, Ind. Crops Prod. 88 (2016) 96–105. https://doi.org/10.1016/j.indcrop.2016.03.002.

[7] K. Ghassemi-Golezani, N. Farhadi, The Efficacy of Salicylic Acid Levels on Photosynthetic Activity, Growth, and Essential Oil Content and Composition of Pennyroyal Plants Under Salt Stress, J. Plant Growth Regul. 41 (2022) 1953–1965. https://doi.org/10.1007/s00344-021-10515-y.

[8] P.S. Vankar, D. Shukla, Biosynthesis of silver nanoparticles using lemon leaves extract and its application for antimicrobial finish on fabric, Appl. Nanosci. 2 (2012) 163–168. https://doi.org/10.1007/s13204-011-0051-y.

[9] C. Baker, A. Pradhan, L. Pakstis, D. Pochan, S.I. Shah, Synthesis and antibacterial properties of silver nanoparticles, J. Nanosci. Nanotechnol. 5 (2005) 244–249. https://doi.org/10.1166/jnn.2005.034.

[10] M. Guzman, J. Dille, S. Godet, Synthesis and antibacterial activity of silver nanoparticles against gram-positive and gram-negative bacteria, Nanomedicine Nanotechnology, Biol. Med. 8 (2012) 37–45. https://doi.org/10.1016/j.nano.2011.05.007.

[11] A. Martirosyan, A. Bazes, Y.-J. Schneider, In vitro toxicity assessment of silver nanoparticles in the presence of phenolic compounds –preventive agents against the harmful effect?, Nanotoxicology. 8 (2014) 573–582. https://doi.org/10.3109/17435390.2013.812258.

[12] K .J. Lee, P.D. Nallathamby, L.M. Browning, C.J. Osgood, X.-H.N. Xu, In Vivo Imaging of Transport and Biocompatibility of Single Silver Nanoparticles in Early Development of Zebrafish Embryos, ACS Nano. 1 (2007) 133–143. https://doi.org/10.1021/nn700048y.

[13] P. Dallas, V.K. Sharma, R. Zboril, Silver polymeric nanocomposites as advanced antimicrobial agents: Classification, synthetic paths, applications, and perspectives, Adv. Colloid Interface Sci. 166 (2011) 119–135. https://doi.org/10.1016/j.cis.2011.05.008.

[14] A.K. Mittal, Y. Chisti, U.C. Banerjee, Synthesis of metallic nanoparticles using plant extracts, Biotechnol. Adv. 31 (2013) 346–356. https://doi.org/10.1016/j.biotechadv.2013.01.003.

[15] T.N. Agaev, A.A. Garibov, S.Z. Melikova, G.T. Imanova, Radiation-Induced Heterogeneous Processes of Water Decomposition in the Presence of Mixtures of Silica and Zirconia Nanoparticles, High Energy Chem. 52 (2018) 145–151. https://doi.org/10.1134/S0018143918020029.

[16] A.A. Garibov, T.N. Agaev, S.Z. Melikova, G.T. Imanova, I. A. Faradjzade, Radiation and catalytic properties of the n-ZrO2–n-Al2O3 systems in the process of hydrogen production from water, Nanotechnol. Russ. 12 (2017) 252–257. https://doi.org/10.1134/S1995078017030077.

[17] G.T. Imanova, T.N. Agayev, S.H. Jabarov, Investigation of structural and optical properties of zirconia nanoparticles by radiation-thermal and thermal methods, Mod. Phys. Lett. 35 (2021) 2150050. https://doi.org/10.1142/S0217984921500500.

[18] I. Ali, G.T. Imanova, X.Y. Mbianda, O.M.L. Alharbi, Role of the radiations in water splitting for hydrogen generation, Sustain. Energy Technol. Assess. 51 (2022) 101926. https://doi.org/10.1016/j.seta.2021.101926.

[19] I. Ali, G.T. Imanova, A.A. Garibov, T.N. Agayev, S.H. Jabarov, et al., Gamma rays mediated water splitting on nano-ZrO2 surface: Kinetics of molecular hydrogen formation, Radiat. Phys. Chem. 183 (2021) 109431. https://doi.org/10.1016/j.radphyschem.2021.109431.

[20] J. McGrady, S. Yamashita, S. Kano, H. Yang, A. Kimura, H. Abe,H2 generation at metal oxide particle surfaces under γ-radiation in water, J. Nucl. Sci. Technol. 58 (2021) 604–609. https://doi.org/10.1080/00223131.2020.1847705.

[21] M-C. Pignié, V. Shcherbakov, T. Charpentier, M. Moskura, C. Carteret, et al., Confined water radiolysis in aluminosilicate nanotubes: the importance of charge separation effects, Nanoscale.13 (2021) 3092–3105. https://doi.org/10.1039/D0NR08948F.

[22] T. Kojima, K. Takayanagi, R. Taniguchi, S. Okuda, S. Seino, T.A. Yamamoto, Hydrogen gas generation from the water by gamma-ray radiolysis with pre-irradiated silica nanoparticles dispersing, J. Nucl. Sci. Technol. 43 (2006) 1287–1288. https://doi.org/10.1080/18811248.2006.9711222.

[23] G.T. Imanova, T.N. Agaev, A.A. Garibov, S.Z. Melikova, S.H. Jabarov, H.V. Akhundzada, Radiation-thermocatalytic and thermocatalytic properties of n-ZrO2-n-SiO2 systems in the process of obtaining hydrogen from water at different temperatures, J. Mol. Struct. 1241 (2021) 130651. https://doi.org/10.1016/j.molstruc.2021.130651.

[24] H. Fang, Y. Pan, M. Yin, L. Xu, Y. Zhu, C. Pan, Facile synthesis of ternary Ti3C2–OH/ln2S3/CdS composite with efficient adsorption and photocatalytic performance towards organic dyes, J. Solid State Chem. 280 (2019) 120981. https://doi.org/10.1016/j.jssc.2019.120981.

[25] J. Ji, L. Zhao, Y. Shen, S. Liu, Y. Zhang, Covalent stabilization and functionalization of MXene via silylation reactions with improved surface properties, FlatChem. 17 (2019) 100128. https://doi.org/10.1016/j.flatc.2019.100128.

[26] X. Li, X. Ma, Y. Hou, Z. Zhang, Y. Lu, et al., Intrinsic voltage plateau of a Nb2CTx MXene cathode in an aqueous electrolyte induced by high-voltage scanning, Joule. 5 (2021) 2993–3005. https://doi.org/10.1016/j.joule.2021.09.006.

[27] X. Zhai, H. Dong, Y. Li, X. Yang, L. Li, et al., Termination effects of single-atom decorated v-Mo2CTx MXene for the electrochemical nitrogen reduction reaction, J. Colloid Interface Sci. 605 (2022) 897–905. https://doi.org/10.1016/j.jcis.2021.07.083.

[28] Y. Gao, Y. Cao, H. Zhuo, X. Sun, Y. Gu, et al., Mo2TiC2 MXene: A promising catalyst for electrocatalytic ammonia synthesis, Catal. Today. 339 (2020) 120–126. https://doi.org/10.1016/j.cattod.2018.12.029.

[29] A. Kudo, Y. Miseki, Heterogeneous photocatalyst materials for water splitting, Chem. Soc. Rev. 38 (2009) 253–278. https://doi.org/10.1039/B800489G.